Acta Crystallographica Section A
Foundations of Crystallography
ISSN 0108-7673

Received 28 August 2002
Accepted 7 November 2002

Domino phase-retrieval algorithm for structure determination using electron diffraction and high-resolution transmission electron microscopy patterns

F. N. Chukhovskii[a] and A. M. Poliakov[b]*

[a]Institute of Crystallography, the Russian Academy of Sciences, 117333 Moscow, Leninsky Prospect 59, Russia, and [b]Department of Materials Science, Moscow Institute of Steel and Alloys, 117279 Moscow, Leninsky Prospect 4, Russia. Correspondence e-mail: poliakov@yahoo.com

Direct-method formalism to determine atomic structures using electron diffraction data is here aimed at a general solution of the phase-retrieval problem, consequently combining electron diffraction (ED) and high-resolution transmission electron microscopy (HRTEM) patterns in a 'domino' fashion. While there are similarities to conventional (kinematical) direct methods, there remain major differences; in particular, owing to the dynamical effects in the data, the ED structure factors prove to be complex and then the positivity of the reconstructed electron density is no longer a valid constraint for 'dynamical' direct methods. Besides, owing to the dynamical effects, heavy atoms no longer dominantly contribute to the HRTEM images. Thus, the 'dynamical' direct-methods concept is based on the phase-retrieval algorithm utilizing both the dynamical ED and the HRTEM data. The fusion of the traditional direct-method technique, which is described here, allows realization of a full-phase restoration of complex structure factors. A numerical example, using the dynamical ED and HRTEM data for $(Ga,In)_2SnO_5$ ceramic, shows that the method is capable of yielding a unique phase-retrieval solution. The clear sense is that the domino transform algorithm proposed works well and represents a valuable method for phasing diffraction patterns in electron structural crystallography using an experiment that is readily performed when the ED and HRTEM data are collected.

1. Introduction

An application of conventional (kinematical) direct methods and refinements for purposes of electron structure determination raises some fundamental problems. There are some simple cases, for instance a surface, where such refinements are legitimate as a good first approximation, but even here correct results require the inclusion of dynamical effects (*e.g.* Marks & Landree, 1998). It is very well established theoretically that even one atom layer of a heavy element such as gold is a 'dynamical' scattering unit (see *e.g.* Buseck *et al.*, 1988; Spence, 1988), so there are no cases with real samples where the kinematical approximation is rigorously valid. While exceedingly thin values such as 2 nm are sometimes reported for sample thickness used in interpreting experimental high-resolution transmission electron-microscopy (HRTEM) images, the actual thickness is certainly larger; the discrepancy is often due to neglecting terms such as sample vibration or beam tilt. At the same time, under some optimal imaging conditions, the HRTEM technique provides real-space information toward crystal structures though HRTEM images in general do not contain true atom positions. On the other hand, to obtain true real-space information concerning atom positions, one may explore the direct methods relying on the diffraction information alone and extracting the unknown phase information among the structure factors (Dorset, 1995; Woolfson & Fan, 1995; Giacovazzo, 1998). Most earlier combinations of HRTEM and direct methods have been tested neglecting dynamical effects in electron diffraction (ED) data, namely, the direct methods have been applied within a kinematical approach (Fan *et al.*, 1991; Hu *et al.*, 1991; Gilmore *et al.*, 1993; Dorset, 1996; Marks *et al.*, 1997).

Noteworthy is the fact that the first quantitative relationships capable of being used for phasing diffraction patterns *via* direct methods were Sayre's equation (Dorset, 1995 and statistical phase invariants (Cochran & Woolfson, 1955; Hauptman, 1982). Switching to a set of structure factors, $\{U(\mathbf{g})\}$, the phase set $\{\psi(\mathbf{g})\}$ with $\psi(\mathbf{g}) = \mathrm{Im}[\ln[U(\mathbf{g})]]$ and $\mathbf{g}$ a reciprocal-lattice vector, could be determined using the iterative transform algorithm based on the Sayre-tangent formula as a convolution equation (namely, $\psi(\mathbf{g}) = \mathrm{Im}[\ln[\Sigma_{\mathbf{h}} U(\mathbf{h})U(\mathbf{g}-\mathbf{h})]]$ with the known set of moduli $\{|U(\mathbf{g})|\}$;

see *e.g.* Dorset, 1995; Giacovazzo, 1998; Landree *et al.*, 1997; for details). For this, the Sayre-tangent formula is relatively exact for point-like atomic structures as long as the atom scatterer positions are not overlapped, which coincides with the basic assumption of the ED channeling approximation (Van Dyck & Op de Beeck, 1996; Sinkler & Marks, 1999; Hu & Tanaka, 1999).

At the same time, the phase information is preserved in the HRTEM images and can be extracted sometimes using the Fourier transform (DeRosier & Klug, 1968; Weirich *et al.*, 1996). Ishizuka *et al.* (1982) have developed the resolution improvement and/or phase correction method first proposed by Hoppe & Gassmann (1968). Combining the information in the electron micrograph and electron diffraction within the weak scattering approximation, they have applied the procedure to the model structure of the crystal of copper perchlorophthalocyanine for determining the phases (signs) of the structure factors.

The prospects for the least-squares refinement (Dorset & Gilmore, 2000) and direct-method technique (Weirich *et al.*, 2000) to decode structural data from an ED experiment was recently reviewed in many cases, in most of which dynamical ED effects were ignored. The work (Sinkler *et al.*, 1998) is developed into ans example, in which the direct methods combining with the Fourier transform of the HRTEM image were used to attempt to solve the phase problem on a sample of $(Ga,In)_2SnO_5$ ceramic.

After that, the two- and three-phase structure invariants, Σ_0 and Σ_2, within the scope of 'dynamical' direct methods were analyzed (Hu *et al.*, 2000; Chukhovskii *et al.*, 2001). It was shown how the relevant success of applying direct methods to dynamical ED data can be understood *via* an 'effective kinematical approximation' since each of the phase conditional probability distributions, Σ_0, defined for a number of $(\mathbf{g}, -\mathbf{g})$ reflection pairs, and the phase conditional probability distribution, Σ_2, defined for a number of $(\mathbf{g}, \mathbf{h}, -\mathbf{g}-\mathbf{h})$ reflection triplets, are proved to display a strong peak in many cases. The above assertion is obtained using the theoretical probability background (Hauptman, 1982) and confirmed by numerical multislice calculations. Particularly noteworthy is the fact that the recovered effective dynamical potential may be similar to the kinematical one but does not have to be and in general will not be.

In this paper, we push the concept of direct methods one step further, and apply it using both two-dimensional ED and HRTEM data sets as constraints for phase restoration. To apply this concept, the iterative transform algorithm, which has at its core the Gerchberg–Saxton algorithm (Gerchberg & Saxton, 1972; see Dainty & Fienup, 1987 as well) and makes the phase-retrieval procedure in a domino fashion, is proposed. We believe that no such iterative transform algorithm for direct phasing of the ED complex structure factors has been previously reported. A prerequisite to solving the problem herein is to elaborate the appropriate numerical algorithm that creates a unique phase restoration. For purposes of this study, some numerical simulations are given for a sample of $(Ga,In)_2SnO_5$ ceramic, which exhibits a convergence property of the domino iterative transform algorithm proposed. In particular, the new algorithm that is described here has been proven to be convergent in the general case of complex structure factors. Noteworthy is the fact that its application can facilitate a true determination of nanometre-size crystal structures combining both the ED and HRTEM data in a sequential domino manner.

2. Problem foundation. Domino iterative transform algorithm combining ED and HRTEM data

Aiming to introduce the necessary mathematical formalism describing the dynamical electron scattering within the scope of the 1s channeling approximation, we will briefly repeat the derivation of the complex structure factors $\{U(\mathbf{g})\}$ first given by Van Dyck & Op de Beeck (1996) and discussed in more detail in Appendix *A* of Hu *et al.* (2000). As discussed in the paper (Hu *et al.*, 2000), we can write a complete solution for the electron wavefunction in a thin crystal as a sum of the two-dimensional channeling eigenstates $\Psi_n(\mathbf{R})$, where $\mathbf{R} \equiv (x,y)$ is a two-dimensional vector perpendicular to the electron-beam direction:

$$\Psi(\mathbf{R}, z) = 1 + \sum_n a_n \Psi_n(\mathbf{R})\{\exp[-i\pi(E_n/E_0)\kappa z] - 1\}. \quad (1)$$

The sum in (1) is over the eigenstates labeled n, with occupations a_n. Each eigenstate as a function of depth z has a characteristic oscillation frequency, which is determined by the channeling (Bloch wave) eigenvalue E_n (E_0 being the incident electron energy and $\kappa = \lambda^{-1}$). For a thin crystal, this series solution can be legitimately truncated after including only the most significant terms [see *e.g.* Appendix *A* in Hu *et al.* (2000) for details]. For moderate values of sample thickness and atomic numbers, a further simplification of (1) can be used for cases in which the atomic columns are well separated in projection so that the atomic potentials do not strongly overlap. In such cases, the lowest lying eigenstate E_j (analogous to the j atomic 1*s* state) mainly contributes to the sum in the right-hand side of (1), so the electron wavefunction may be written as (Van Dyck & Op de Beeck, 1996)

$$\Psi(\mathbf{R}, z) = 1 + 2i\sum_{j=1}^{J} a_j \Psi_j(\mathbf{R} - \mathbf{R}_j)\exp\{-i\pi(E_j/2E_0)\kappa z\} \times \sin\{\pi(-E_j/2E_0)\kappa z\}, \quad (2)$$

where now the sum is over the j atomic positions.

We will now use this form and switch to reciprocal space, the standard space used in structure analysis. The structure factor for the $\mathbf{g}$ reflection takes the form

$$U(\mathbf{g}) \equiv iF_{\mathbf{g}} = i\sum_{j=1}^{J} F_{j\mathbf{g}} \exp(-i2\pi\mathbf{g}\cdot\mathbf{r}_j), \quad (3)$$

where

$$F_{j\mathbf{g}} = 2V_j(\mathbf{g})\exp\{-i\pi(E_j/2E_0)\kappa z\}\sin\{-\pi(E_j/2E_0)\kappa z\} \quad (4)$$

is the complex atomic scattering amplitude of the atom labeled j, $\mathbf{r}_j$ is its position vector and J is the number of atomic columns

in the two-dimensional unit cell. $V_j(\mathbf{g})$ is the Fourier transform of $\Psi_j(\mathbf{R}-\mathbf{R}_j)$, to a first approximation the *kinematical* single-atom structure factor.

Generally, addressed to nanometre-size structural electron crystallography, the problem of phase retrieval is related to the complex structure-factor set $\{U(\mathbf{g})\}$ and the HRTEM image $I(\mathbf{x})$. They are formed as a result of the plane-wave propagation through an *electron optical system* consisting of selected-area apertures and focusing lens taking into account all likely aberrations (*e.g.* defocus, spherical aberration and so on). The focused electron wave is imaged onto the two-dimensional (2D) arrays of detectors that specifically measure intensity either in the back focal or in the image plane, respectively. Intensities measured in the back focal plane are referred to the ED magnitudes $\{|U(\mathbf{g})|\}$, with diverse reciprocal-lattice vectors $\mathbf{g}$, whereas the intensity distribution $I(\mathbf{x})$ in the image plane is the modulus squared of the Fourier transform of the complex structure-factor set $\{U(\mathbf{g})\}$. The 2D periodical function $I(\mathbf{x})$ is the HRTEM image of the crystal structure. From the mathematical viewpoint, the data array of $\{|U(\mathbf{g})|\}$ (and the data array $\{A(\mathbf{x})\}$ as well, with $A(\mathbf{x}) \equiv [I(\mathbf{x})]^{1/2}$) is non-convex. The non-convexity of both the underlying sets, $\{|U(\mathbf{g})|\}$, $\{A(\mathbf{x})\}$, is a main obstacle to applying the Gerchberg–Saxton-type algorithm for phasing diffraction patterns directly.

On the other hand, it is physically reasonable, as well as mathematically precise, to consider that the phase-retrieval problem amounts to determining the phases of the complex structure factors from both the arrays ${}_{(N)}\{|U(\mathbf{g})|\}$, ${}_{(N)}\{A(\mathbf{x})\}$, which may be measured in the back focal plane and the image plane, respectively, and N is the array rank (the corresponding array size is equal to $N \times N$).

Thus, in order to overcome the fundamental non-convexity limitation and, as a result, to avoid numerous redundant solutions, we will trade off the known Gerchberg–Saxton method onto the new Gerchberg–Saxton-type algorithm for phase determination in a sequential 'domino' fashion.

Specifically, let us introduce the oblique-angled *selected-area* constraint sets of ${}_{(\nu)}\{|U(\mathbf{g})|, A(\mathbf{x})\}$ for the consecutive values of $\nu = 2, 3, 4, \ldots, N$ [$U(\mathbf{g})_{\mathbf{g}=0}$ is assumed to be unity for any ν]. If the oblique-angled selected-area array rank ν is considered as a fixed iteration number, the numerical algorithm scheme search takes the form

$$\begin{aligned}
{}_{(\nu)}M_{k+1}(\mathbf{x}) &= {}_{(\nu)}A(\mathbf{x})\exp[i_{(\nu)}\varphi_k(\mathbf{x})]\\
{}_{(\nu)}|U_{k+1}(\mathbf{g})| &= |\text{Inverse Fourier}\,[{}_{(\nu)}M_{k+1}(\mathbf{x})]|\\
{}_{(\nu)}\psi_{k+1}(\mathbf{g}) &= \text{Im}[\ln[\text{Inverse Fourier}\,[{}_{(\nu)}M_{k+1}(\mathbf{x})]]]\\
{}_{(\nu)}U_{k+1}(\mathbf{g}) &= |{}_{(\nu)}U(\mathbf{g})|\exp[i_{(\nu)}\psi_{k+1}(\mathbf{g})]\\
{}_{(\nu)}A_{k+1}(\mathbf{x}) &= |\text{Fourier}\,[{}_{(\nu)}U_{k+1}(\mathbf{g})]|\\
{}_{(\nu)}\varphi_{k+1}(\mathbf{x}) &= \text{Im}[\ln[\text{Fourier}\,[{}_{(\nu)}U_{k+1}(\mathbf{g})]]],
\end{aligned} \tag{5}$$

where we calculate the $(k+1)$th phase sets of ${}_{(\nu)}\{\psi_{k+1}(\mathbf{g}), \varphi_{k+1}(\mathbf{x})\}$ by use of the preceding kth ones ${}_{(\nu)}\{\psi_k(\mathbf{g}), \varphi_k(\mathbf{x})\}$, and keeping in mind that the ED and HRTEM sets of ${}_{(\nu)}\{|U(\mathbf{g})|, A(\mathbf{x})\}$ are *a priori* fixed and do not depend on the cycle value of k over all the iteration processes of ν (*e.g.* they are equal to the 'experimental' values). The two figures of merit (FOM) related to the reciprocal space, $R^{(\nu)}$, and real space, $X^{(\nu)}$, are evaluated at each cycle over k:

$$\begin{aligned}
R^{(\nu)}_{k+1} &= \nu\Sigma_{\mathbf{g}}||{}_{(\nu)}U_{k+1}(\mathbf{g})| - |{}_{(\nu)}U(\mathbf{g})||/[\Sigma_{\mathbf{g}}|{}_{(\nu)}U(\mathbf{g})|^2]^{1/2},\\
X^{(\nu)}_{k+1} &= \nu\Sigma_{\mathbf{x}}|{}_{(\nu)}A_{k+1}(\mathbf{x}) - {}_{(\nu)}A(\mathbf{x})|/[\Sigma_{\mathbf{x}(\nu)}I(\mathbf{x})]^{1/2}.
\end{aligned} \tag{6}$$

For reference, ${}_{(\nu)}\psi_k(\mathbf{g})$ is the given phase of the complex structure factor ${}_{(\nu)}U_k(\mathbf{g})$ at the beginning of each cycle k, and ${}_{(\nu)}\psi_{k+1}(\mathbf{g})$ is the new phase calculated at the end of the same cycle. The calculated phase set of ${}_{(\nu)}\{\psi_{k+1}(\mathbf{g})\}$ is then fed back into the cycle iteration fashion according to the 'flow' equation (5), $k = 1, 2, 3, \ldots, K$, and the range value K is chosen to be fixed.

Our main focus is on the fact that some important restrictions are imposed onto the phase set of ${}_{(\nu+1)}\{\psi_k(\mathbf{g})\}$, specifically, the phase set of ${}_{(\nu+1)}\{\psi_k(\mathbf{g})\}$ contains the subset of ${}_{(\nu)}\{\psi(\mathbf{g})\}$, with the array size of $\nu \times \nu$, determined within the preceding iteration of ν. And, clearly, the other elements of the phase set of ${}_{(\nu+1)}\{\psi_k(\mathbf{g})\}$ are chosen to be random in the range of $(-\pi, \pi)$ for the first cycle, $k = 1$, only.

Loosely speaking, the principal idea of the domino phase-retrieval method is to obtain the phase fit for the complete structure-factor set $\{U(\mathbf{g})\}$ sequentially step by step starting from the first subsets ${}_{(2)}\{|U(\mathbf{g})|\}$, and ${}_{(2)}\{A(\mathbf{x})\}$, each of them has the rank size 2, and for every combined subset ${}_{(\nu)}\{|U(\mathbf{g})|, A(\mathbf{x})\}$, $\nu = 2, 3, 4, \ldots, N$, the standard Gerchberg–Saxton iteration procedure is applied.

Complementarily, we then use the phase consistency check factor (a 'correctness' factor)

$$C^{(\nu)}_{k+1} = 0.5\Sigma'_{\mathbf{g}}|{}_{(\nu)}U_{k+1}(\mathbf{g}) - {}_{(\nu)}U(\mathbf{g})|/\Sigma'_{\mathbf{g}}|{}_{(\nu)}U(\mathbf{g})| \tag{7}$$

that is calculated in a process of numerical simulations for all the values of k, and the sum, Σ', taken over all the reflections except $\mathbf{g} = 0$.

The $C^{(\nu)}_k$ factor being calculated at each iteration step ν as a function of k provides a means of monitoring the progress of the code during the entire iteration procedure. The numerical phase simulation procedure [see equations (5)–(7)] from $\nu = 2$ until the final iteration value of N is iterated guiding the phases as long as the values of $R^{(N)}$ and $X^{(N)}$ reduce to the consensual estimates. Note that equations (6) play the role of penalty functions for constraining likely atomic structure solutions operating with the calculated and *a priori* known ED and HRTEM data.

The 'domino' idea for the iterative transform algorithm rests on the restriction of the total number of the likely solutions for the ED and HRTEM input data set of ${}_{(2)}\{|U(\mathbf{g})|, A(\mathbf{x})\}$, where $\nu = 2$, that launch the general iteration procedure. It is easy to show that in the case of the input iteration value of $\nu = 2$ there are eight different solutions for the phase set of ${}_{(2)}\{\psi(\mathbf{g})\}$, more precisely, there are the four different pairs of the complex conjugate structure factors, one of which is referred to as a true solution [recall that $\psi(\mathbf{g})_{\mathbf{g}=0} \equiv 0$]. Going on from the iteration of $\nu = 2$ until the final iteration N *via* the consecutive oblique-angled selected-area iterations, the true phase solution holds up to some numerical uncer-

tainties depending on the final iteration number N, whereas other redundant solutions can be readily detected yielding inappropriate values of FOM. Presumably, numerical uncertainties of the 'correct' phases increase with increasing iteration number (the reflection array rank) ν, which might be compensated for by enlarging the cycle range value of K.

Below, the domino iterative transform algorithm above described is tested numerically with simulated input ED and HRTEM data and the true solution of the $(Ga,In)_2SnO_5$ crystal structure.

3. Numerical simulations. Results and discussion

The test case we consider is a centrosymmetric structure of the ceramic $(Ga,In)_2SnO_5$. The structure is monoclinic with a = 1.169, b = 0.317, c = 1.073 nm and β = 99.00°. The atom positions within the unit cell obtained from direct methods and neutron diffraction are presented in Sinkler *et al.* (1998), the projected two-dimensional structure of $(Ga,In)_2SnO_5$ is shown in Fig. 1. The incident electron beam propagates along the b axis and the accelerating voltage is 300 kV.

The complex structure factors related to the proper dynamical ED pattern for $(Ga,In)_2SnO_5$ were calculated using the 1s-state channeling approach (see *e.g.* Hu *et al.*, 2000; Chukhovskii *et al.*, 2001 for details) for 4.121 nm thickness (Fig. 2) and 7.291 nm thickness (Fig. 3) along the b axis. The standard images calculated using the above values of thickness and 0.01 nm resolution are shown in Fig. 2(a) and Fig. 3(a), respectively.

To illustrate the convergent features of the new algorithm guiding the phase determination based upon the flow equation (5), the data sets of ${}_{(\nu)}\{|U(\mathbf{g})|, A(\mathbf{x})\}$ were explored in a sequential manner from the initial value of $\nu = 2$ up to the two different final iteration values of N, namely $N = 20$ and $N = 40$,

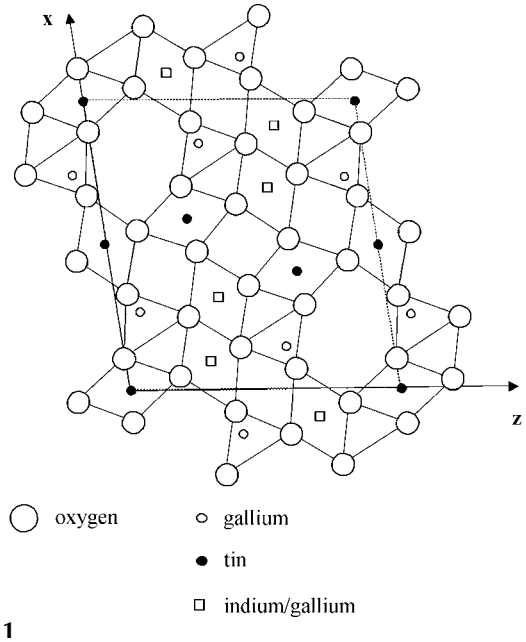

Figure 1
Structure of $(Ga,In)_2SnO_5$ viewed along $[0\bar{1}0]$.

respectively. Figs. 2(b) and (c) and Figs. 3(b) and (c) show the calculated unit-cell images, ${}_{(20)}I(\mathbf{x})$ and ${}_{(40)}I(\mathbf{x})$, obtained as the modulus squared of the Fourier transform of the unique phase-recovered structure-factor sets of ${}_{(20)}\{U(\mathbf{g})\}$ and ${}_{(40)}\{U(\mathbf{g})\}$ using the domino iterative transform algorithm detailed above. It is interesting that in the case of the iteration number N = 20 the real-space unit-cell images [see Figs. 2(b), 3(b)] do not keep the centrosymmetry property as a result of the insufficient spatial resolution of order of 0.05 nm (it should be noted that the atom positions need not coincide with nodes of a numerical net) rather than as aa result of the phase-retrieval solution based on the present iteration transform algorithm application. As an example, Fig. 4 shows the behavior of the calculated parametric plots of the R-FOM *versus* a 'correctness' C factor [*cf.* equations (6)–(7)]. It is found that, in the case of the domino iterative transform algorithm application to the solution of $(Ga,In)_2SnO_5$, the calculated R-FOM and C factor achieve the appropriate values of order of 10^{-5} and 10^{-7} for the cycle range K = 100

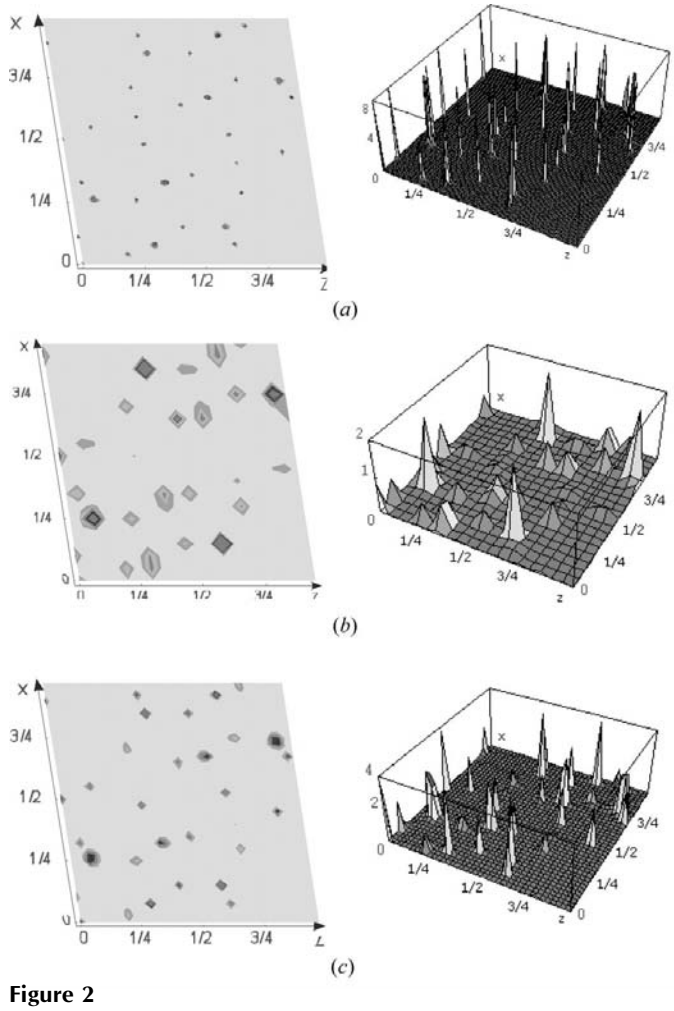

Figure 2
Images of $(Ga,In)_2SnO_5$ structure (2D and 3D plots) showing the phase-retrieval solution for the iteration range of N = 20 in (b) and the phase-retrieval solution for the iteration range of N = 40 in (c) in comparison with the standard gauge image in (a) calculated for the iteration range of N = 100. The cycle range of K is 1000. The sample thickness along the b axis is 4.121 nm.

used for the calculated images shown in Figs. 3(*b*), (*c*). It is worth noticing that, in the case of the cycle range value of K = 1000 taken for the numerical simulation of the real-space structure images in Figs. 2(*b*), (*c*), the corresponding values of *R*-FOM and *C* factor are practically equal to zero (less than 10^{-27}).

Thus, with the trends of the *R*-FOM reduction observed and confirmed by the *C*-factor reduction behavior, the domino iteration transform algorithm by consecutively combining the ED and HRTEM data gives a good convergence in the phase-retrieval procedure. It should be noted that, depending on the initial random phases of an input phase set of complex structure factors, for the initial iteration value of $\nu = 2$ the numerical code proposed generates redundant solutions too. Fortunately, they can be effectively discriminated by imposing a 'break' condition incorporated within the complete iteration procedure, for instance, by choosing inappropriate barrier values of *R*-FOM equal to 0.01.

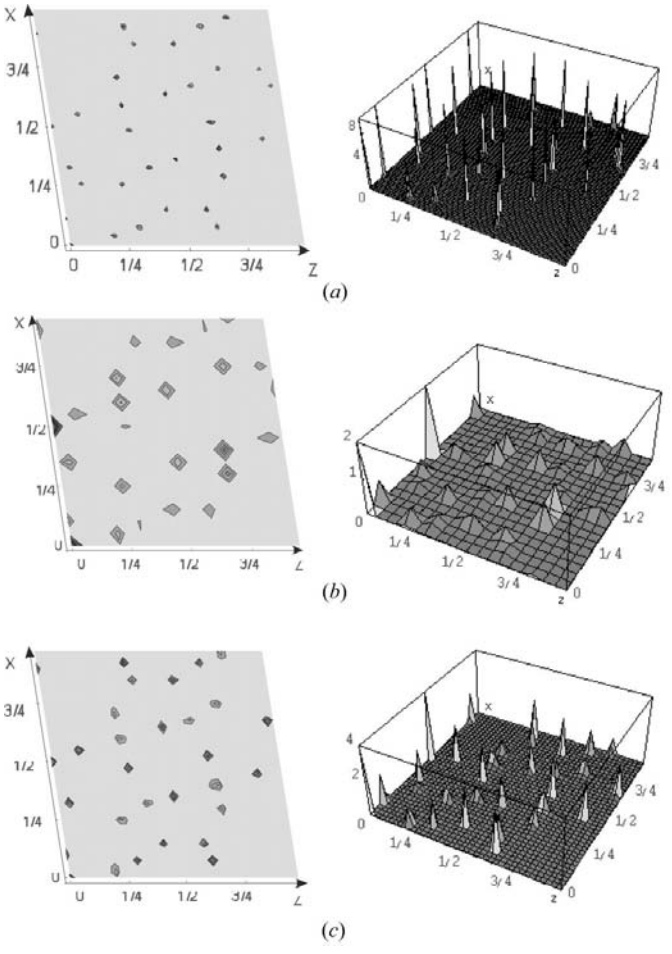

Figure 3
Images of $(Ga,In)_2SnO_5$ structure (2D and 3D plots) showing the phase-retrieval solution for the iteration range of N = 20 in (*b*) and the phase-retrieval solution for the iteration range of N = 40 in (*c*) in comparison to the standard gauge image in (*a*) calculated for the iteration range of N = 100. The cycle range K is 100. The sample thickness along the *b* axis is 7.291 nm.

4. Concluding remarks

In this paper, the goal of our study is to justify the application of the domino iterative transform algorithm detailed above for phasing diffraction patterns. The main point of the new numerical code is that the latter provides the robust unambiguous iterative procedure, at least for two-dimensional phasing problems, by operating with the ED and HRTEM data as the physically measured constraints. Specifically, in what is referred to as a general phase-retrieval problem, the present domino method can be considered as a synthesis of the diverse direct methods, which are widely explored for electron structure determination (Dorset, 1995; Weirich *et al.*, 2000). Numerical simulations of the crystal model structure show that, unlike the direct methods earlier utilized, the routine algorithm by using the composite input ED and HRTEM data sets in a domino fashion is reasonable from the physical viewpoint and does not depend on any assumptions (*e.g.* the weak-scattering approximation) and primary models of the crystal structure in question to restore phases of the complex structure factors. Generally, the present algorithm code is proven to be convergent and successful for solving phase-retrieval problems (at least in the case of the two-dimensional data sets). It seems likely that even complicated crystal structures, for which parts of some reflections are not available to be measured, can be solved in this way by extending the feasible complex structure factors to unmeasurable ones by means of the Sayre equation.

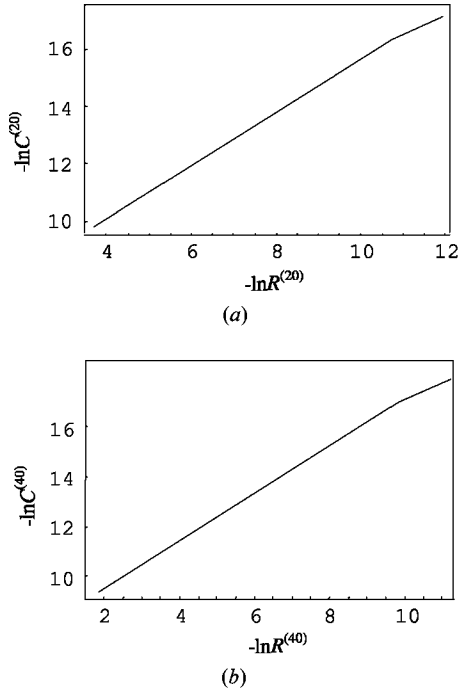

Figure 4
Plot of the factor $-\ln R$ *versus* a 'correctness' factor $-\ln C$ calculated within the final set of phase assignments using the two ranges of structure factors: (*a*) N = 20, (*b*) N = 40 (the cycle range of K = 100). The sample thickness along the *b* axis is 7.291 nm. The curved parts with the largest ($-\ln R$) and ($-\ln C$) values indicate that the present phase-retrieval algorithm provides a full restoration of phases.

A few final comments are appropriate here about the implementation of the present algorithm code to the practical structural analysis using ED and HRTEM data. As is pointed out, the ED dynamical effects were taken into consideration within the scope of a 1*s* electron channeling approach for the input ED data. It needs to be remembered that the validity and application prospect of the domino phase-retrieval algorithm presented are closely related to the ED being dominated by 1*s* channeling states. This is only true for moderate values of sample thickness and atomic numbers. In addition to sample thickness, the accelerating voltage is another adjustable parameter. As the voltage becomes higher, there are more strongly bound states (*e.g.* 2*s*, 3*s*), which complicate the ED (Hu *et al.*, 2000). Yet there are many structures where 2*p* states are important if the sample is tilted off the zone axis. The question of whether the domino phase-retrieval algorithm has any validity in these cases remains as a topic for future research.

Also, testing the present algorithm code, we did not include the aberration phase distortions of the electron optical system, the values of which are in general known *a priori* to form relevant HRTEM images (*cf*. Spence, 1988) and we ignored a possible thickness variation within the sample area selected, albeit the latter might be minimized using the convergent-beam patterns.

With these confines of the input ED and HRTEM data sets, we do not claim anything except that the domino algorithm code for the phase retrieval of structure factors is really convergent and works well. How well it will work in practice, particularly using the input experimental ED and HRTEM data, remains to be seen and is then of special interest for future work.

It should once more be stated in conclusion that the convergent feature and feasibility of the numerical solution of the crystal model structure tested in the general case of complex structure factors imply that direct methods may be properly modified to facilitate further the practical electron structure analysis, particularly by applying the domino iterative transform algorithm technique, a good topic for future work.

One of authors (FNC) gratefully acknowledges J. J. Hu, L. D. Marks and W. Sinkler for stimulating discussions of direct methods addressed to phasing diffraction patterns for purposes of electron structure determination.

References

Buseck, P. R., Cowley, J. M. & Eyring, L. (1988). Editors. *High-Resolution Transmission Electron Microscopy and Associated Techniques.* Oxford University Press.
Chukhovskii, F. N., Hu, J. J. & Marks, L. D. (2001). *Acta Cryst.* A**57**, 231–239.
Cochran, W. & Woolfson, M. M. (1955). *Acta Cryst.* **8**, 1–12.
Dainty, J. & Fienup, J. (1987). *Image Recovery: Theory and Application*, edited by H. Stark. New York: Academic Press.
DeRosier, D. J. & Klug, A. (1968). *Nature (London)*, **217**, 130–134.
Dorset, D. L. (1995). *Structural Electron Crystallography.* New York: Plenum Press.
Dorset, D. L. (1996). *Acta Cryst.* B**52**, 753–758.
Dorset, D. L. & Gilmore, C. J. (2000). *Acta Cryst.* A**56**, 62–67.
Fan, H.-F., Xiang, S. B., Li, F. H., Pan, Q., Uyeda, N. & Fujiyoshi, Y. (1991). *Ultramicroscopy*, **36**, 361–365.
Gerchberg, R. W. & Saxton, W. O. (1972). *Optik (Stuttgart)*, **35**, 237–244.
Giacovazzo, C. (1998). *Direct Phasing in Crystallography. Fundamentals and Applications.* Oxford University Press.
Gilmore, C. J., Shankland, K. & Bricogne, G. (1993). *Proc. R. Soc. London Ser. A*, **442**, 97–101.
Hauptman, H. (1982). *Acta Cryst.* A**38**, 632–641.
Hoppe, W. & Gassmann, J. (1968). *Acta Cryst.* B**24**, 97–107.
Hu, J. J., Chukhovskii, F. N. & Marks, L. D. (2000). *Acta Cryst.* A**56**, 458–469.
Hu, J. J., Li, F. H. & Fan, H. F. (1991). *Ultramicroscopy*, **41**, 387–391.
Hu, J. J. & Tanaka, N. (1999). *Ultramicroscopy*, **80**, 1–5.
Ishizuka, K., Miyazaki, M. & Uyeda, N. (1982). *Acta Cryst.* A**38**, 408–413.
Landree, E., Collazo-Davila, C. & Marks, L. D. (1997). *Acta Cryst.* B**53**, 916–922.
Marks, L. D. & Landree, E. (1998). *Acta Cryst.* A**54**, 296–305.
Marks, L. D., Plass, R. & Dorset, D. L. (1997). *Surf. Rev. Lett.* **4**, 1–4.
Sinkler, W. & Marks, L. D. (1999). *Ultramicroscopy*, **75**, 251–268.
Sinkler, W., Marks, L. D., Edwards, D. D., Mason, T. O., Pöppelmeier, K. R., Hu, Z. & Jorgensen, J. D. (1998). *J. Solid State Chem.* **136**, 145–149.
Spence, J. C. H. (1988). *Experimental High-Resolution Electron Microscopy.* Oxford University Press.
Van Dyck, D. & Op de Beeck, M. (1996). *Ultramicroscopy*, **64**, 99–107.
Weirich, T. E., Ramlau, R., Simon, A., Hovmöller, S. & Zou, X. D. (1996). *Nature (London)*, **382**, 144–146.
Weirich, T. E., Zou, X. D., Ramlau, R., Simon, A., Cascarano, G. L., Giacovazzo, C. & Hovmöller, S. (2000). *Acta Cryst.* A**56**, 29–35.
Woolfson, M. & Fan, H.-F. (1995). *Physical and Non-Physical Methods of Solving Crystal Structures.* Cambridge University Press.